JOURNAL OF COASTAL AND HYDRAULIC STRUCTURES

Vol. 6, 2026, 54

Maximum influence of wind on wave overtopping at rubble mound breakwaters under oblique wave attack

Maria Sklia [1] and Marcel R.A. van Gent [1*]

Abstract

Especially for coastal structures with a protruding crest wall, wind affects wave overtopping because the crest wall can cause a vertical wave motion above the crest which is susceptible to wind. Earlier studies indicate that wind can increase wave overtopping discharges up to about a factor 5 for coastal structures under perpendicular wave attack. This study investigates the maximum influence of wind on wave overtopping at rubble mound structures under oblique wave attack. To analyse the influence of the wave angle on the maximum influence of wind on wave overtopping, physical model tests in a wave basin have been performed.

The maximum influence of wind is determined under the assumption that all water that exceeds the top of the crest wall would be blown over the crest by onshore wind. The ratio of the total overtopping volume with onshore wind to the total overtopping volume for the same wave condition without wind, provides the maximum influence factor of wind. To obtain the volume of water that exceeds the top of the crest wall, a rotating paddle wheel is employed that transports all water reaching the top of the crest wall to the leeside of the structure.

In addition to earlier studies on the influence of wind on wave overtopping not only the effect of oblique waves on wave overtopping discharges is investigated, but also effects of wind on overtopping volumes in individual overtopping events are analysed.

Results show that for oblique wave incidence, the effect of onshore wind can increase the amount of overtopping significantly. It is confirmed that the influence of wind is more pronounced in conditions with low overtopping discharges. This trend has been shown to be accurate for the description not only of the mean overtopping discharge, but of individual overtopping events as well.

Based on the present tests, the method to account for the maximum influence of wind on wave overtopping discharges has been extended by incorporating the effects of oblique waves. Using this in combination with existing methods to estimate wave overtopping in absence of wind, enables estimates of the actual wave overtopping in real life situations.

[1] Deltares and Delft University of Technology, Delft, The Netherlands
[*] marcel.vangent@deltares.nl

Research Article. Submitted: 4 November, 2025. Reviewed: April 3, 2026. Accepted after double-anonymous review: 17 June, 2026. Published: 14 July 2026.

DOI: 10.59490/jchs.2026.0054

Cite as: Sklia, M. and Van Gent, M.R.A. (2026): Maximum influence of wind on wave overtopping at rubble mound breakwaters under oblique wave attack, Journal of Coastal and Hydraulic Structures, 6, https://doi.org/10.59490/jchs.2026.0054

ISSN: 2667-047X online

Keywords

Wave overtopping, Coastal structures, Rubble mound breakwaters, Wind, Oblique waves, Crest wall, Wave basin tests

1 Introduction

Designing a coastal structure involves the consideration of many environmental forcing mechanisms that can compromise the structure's integrity. A typical example of a forcing mechanism that is sometimes ignored in the design process is the influence of wind on wave overtopping. Ignoring this influence can lead to a less safe design, especially in cases where land use landwards includes either water-sensitive infrastructure or a harbour, where ensuring tranquil mooring conditions of vessels is essential.

Physical model facilities for coastal engineering applications traditionally apply Froude scaling laws to preserve hydraulic similarity between model and prototype structure. In that sense, discharge can be scaled up to prototype and used in the design of the structure. Froude scaling law does not hold for wind, hence, wind cannot be simulated in the lab within a context of a meaningful scaling relationship. Alternative approaches, such as field campaigns or numerical models, also have drawbacks with respect to measuring the influence of wind on wave overtopping in particular. Field campaigns are costly and scarce, and the hydraulic conditions cannot be controlled and generally do not include wave conditions close to the design conditions. Using field measurements it would be nearly impossible to estimate the additional amount of water that overtops solely due to wind, as a storm event cannot be reproduced and the influence of wind on wave overtopping cannot be isolated.

Over about 50 years, it is widely accepted among the coastal engineering community that wind can increase wave overtopping. For instance, Jensen (1984) mentioned that wind-induced spray obstructed usage of reclaimed areas behind breakwaters, or, in the case of adjacent road infrastructure, that the effect of wind was larger for smaller relative wave heights (H_s/R_c), while the influence ceased for higher water levels and rougher sea states. Goda (1985, 2010) referred to the influence of wind on the amount of wave overtopping, stating that it is not negligible and that it is believed that this influence is higher in the low overtopping regime. EurOtop (2018) reported that the mean discharge can increase up to four times, whereas for green water, the influence of wind on wave overtopping becomes less relevant.

Sibul and Tickner (1956) seem to be the first to perform tests in wind-wave tunnels, steering monochromatic waves, and investigated the influence of wind on runup and overtopping at dykes. The first guideline with respect to the added effect of wind on overtopping rates seems to be the one provided in the Shore Protection Manual (SPM, 1984), although the source and reasoning behind that expression are unclear. The manual states that the formulation was not derived based on laboratory experiments or field measurements. In that expression, the wind influence factor depends on the wind speed, which is accounted for with a scaling coefficient, w_f, the structure's seaward slope, the freeboard, and a fictitious runup level. It is mentioned that the increase of overtopping discharge also depends on the wind direction with respect the normal axis to the structure (perpendicular attack). Wind influence factors reaching a maximum of 1.55 for wind speeds of 30 miles per hour for a vertical structure, and a maximum factor of 3.2 for wind speeds of 60 miles per hour or higher, are referred to in the manual.

Hans de Waal introduced a methodology to model the maximum effect of wind on wave overtopping at vertical seawalls (De Waal et al., 1996). That methodology aimed to assess the maximum effect of wind on mean wave overtopping discharge by using a rotating paddle wheel that would transport all the water that reaches above the crest wall level landward, as if onshore wind of sufficient intensity were present. In the tests reported in De Waal et al. (1996), the maximum influence of wind was assessed in terms of the mean overtopping discharge. The maximum wind effect was defined as the ratio of the mean discharge measured with the paddle wheel to the mean discharge in ordinary overtopping tests without paddle wheel, and during that campaign reached a maximum influence factor of wind of $\gamma_w = 3.2$. Wolters and Van Gent (2007) performed wave flume experiments for dikes and rubble mound breakwaters with crest walls. The rotation of the paddle wheel was optimised so that the speed was neither too fast nor too slow to effectively capture and transport the water that exceeded the crest level. The maximum wind effect for dikes and rubble mound breakwaters was quantified in line with results by De Waal et al. (1996) for caisson breakwaters. The maximum measured influence factor was 4.7 for rough slopes. The main conclusions of that study were that the influence of wind increases for smaller overtopping discharges and for increasing freeboard.

Experiments in wind-wave tunnels have been conducted by several researchers since the 1990s, for instance, Ward (1994, 1996), Medina (1998) and Gonzalez-Escriva (2006). Two issues arise in such applications. First, as wind does not scale with Froude laws, it is uncertain how to upscale wind speeds tested in the lab back to prototype conditions, and second, the setup of a wind-wave tunnel could lead to streamline contraction above the structure, which might result in model effects — for instance, overestimation of wave runup. Van Gent et al. (2024) developed a formula (Eq.1) to predict the maximum effect of wind on wave overtopping on dikes and breakwaters with crest walls, based on the physical model tests using the same paddle wheel as Wolters and Van Gent (2007), with tested range of seaward slopes from 1:2 to 1:6 for both breakwaters and dikes with crest walls. This formula accounts for the dependency of the wind influence factor on the discharge itself and the relative height of the protruding part of the crest wall (h_c), leading to zero influence of wind in the absence of a protruding crest wall. The approach used in that study to account for wind effects on wave overtopping makes use of an influence factor (*i.e.*, the ratio of the mean discharge under maximum wind influence to the discharge without wind), which allows pre-existing "wind-free" overtopping estimation methods to be used while incorporating wind in a straightforward manner.

$$\gamma_w = 1 + 0.075 \frac{h_c}{H_{m0}} (q^*)^{-0.3} \tag{1}$$

The influence of wind on wave overtopping has also been studied numerically at full scale. For instance, a numerical investigation on wind-induced wave overtopping at a seawall was conducted by Di Leo et al. (2022) using the shear stress exerted on the water surface in a single-fluid approach. Results showed that the influence of wind is pronounced in the low overtopping discharges. As the discharge decreases, wind increasingly controls overtopping, highlighting the importance of wind in the so-called white overtopping, where overtopping occurs mainly as airborne spray rather than compact water flow. Under these conditions, onshore wind influences significantly the landward transport of spray. Peng and Zou (2011) investigated numerically the spatial distribution of overtopping events in the leeside of coastal structures and found their observations to agree with existing experimental measurements. A notable study on overtopping spray which used experimental methods as the primary research tool is the one by Chen et al. (2023). That study investigated the characteristics of droplets formed after different types of wave impacts on a seawall using a high-speed camera. The study illustrated a sequence of physical processes with respect to the formation of spray during overtopping as follows: wave impact, air entrainment and bubble generation, jet formation, break up and atomisation, spray cloud and droplet trajectories onshore in presence of wind. The authors recommended a formula to predict the maximum height of the spray at 'splash overtopping' as well. Baines et al. (2024) investigated in a physical model campaign the spray-induced downfall pressures acting on the deck of coastal structures which appeared to be significant even for locations further away from the primary point of wave impact on the structure, posing the deck structure at the risk of structural damage, due to a forcing not originally accounted for in the design.

Estimates of wave overtopping discharges without wind are generally based on tests in wave flumes and basins, or on empirical equations based on such tests. In addition, numerical modelling can be used to estimate wave overtopping (e.g. Chen et al., 2021, 2022; Jin et al., 2022; Irías Mata and Van Gent, 2023; and Stagnitti et al., 2023). Empirical expressions for overtopping discharges are also available in manuals such as TAW (2002) and EurOtop (2018). However, these guidelines are outdated for estimates of mean wave overtopping discharges at rubble mound breakwaters due to new knowledge. This includes insights into the influence of shallow foreshores (e.g. De Ridder et al., 2024), the influence of a berm in the seaward slope or a crest wall (e.g. Van Gent et al., 2022), the influence of roughness (e.g. Eldrup et al., 2022; Pepi et al., 2022), oblique wave attack (e.g. Van Gent and Van der Werf, 2019; Van Gent, 2022), or a second wave field in addition to the primary wave field (e.g. Van der Werf and Van Gent, 2018). In addition to such methods, data-driven methods to estimate wave overtopping discharges are available (e.g. Van Gent et al., 2007 and Den Bieman et al., 2021). The most recent guidelines for estimates of wave overtopping discharges at rubble mound breakwaters are provided in Van Gent et al. (2025). The effects of wind on wave overtopping exist in these guidelines (Van Gent et al., 2025) but Eq.1 included therein does not account for the potential influence of oblique waves on the influence of wind on wave overtopping, which is the objective of the present study.

As mentioned above, the main objective of this study is to investigate how oblique wave incidence can affect wind-enhanced wave overtopping. In that sense, the findings of this work can improve the current understanding and offer design guidance that previously considered the increase of wave overtopping due to the presence of wind only owing to normal wave attack. Incorporating wind effects on overtopping during oblique wave incidence in engineering practice mandates a good understanding of the physical processes involved therein, which is presented in the following paragraph. In addition to the analysis for overtopping discharges, an analysis is presented in this study about the wind influence on wave overtopping volumes, i.e., based on individual overtopping events. Improved prediction of these combined effects of wind, foreshore types, structure configuration, etc., on wave overtopping supports the design of safer coastal and port structures and strengthens operational decision-making during extreme events.

By differentiating between four distinguishable scenarios, the top-view sketched in Figure 1 illustrate the potential effects of wind for perpendicular waves and for oblique waves. The cases presented in Figure 1 are: (i) Upper left: Overtopping with No Wind and Perpendicular waves (NWP) and overtopping (OT) discharge: $q(H_{m0}, \beta=0°)$, (ii) Upper right: Overtopping with Wind and Perpendicular waves (WWP) and OT discharge: $\gamma_w * q(H_{m0}, \beta=0°)$, iii) Lower left: Overtopping with No Wind and Oblique Waves (NWO) and OT discharge: $q(H_{m0}, \beta=45°)$ and iv) Lower right: Overtopping with Wind and Oblique Waves (WWO) and OT discharge: $\gamma_w * q(H_{m0}, \beta=45°)$. Figure 1 illustrates that upward-directed water can fall down at locations other than the original location (red dot), hypothetically indicated with ellipses under the four scenarios mentioned above. Onshore wind (effect indicated with the green arrows in Figure 1) can cause the amount of water reaching the rear side of the crest wall (blue line in Figure 1) during oblique wave attack (lower panels) to be smaller than during perpendicular wave attack (upper panels), thus the influence factor of wind γ_w can be smaller for oblique wave attack.

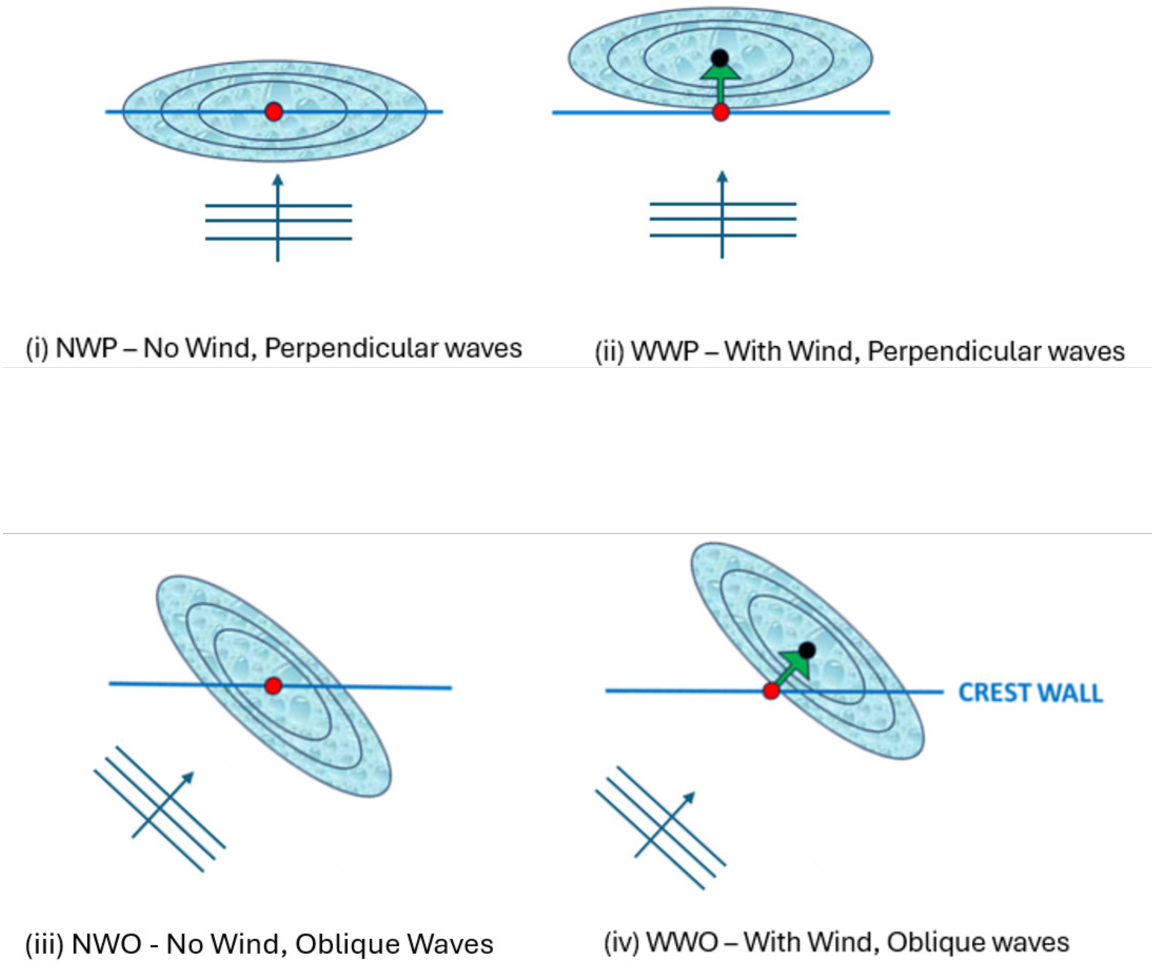

Figure 1: Sketch (top-view) illustrating the original location of a water droplet immediately after flow separation and formation of overtopping jet at the crest wall (red dot) and potential location of the final fall location of this water droplet indicated by the cyan ellipses. Cases illustrated (i) Overtopping with no wind influence and under perpendicular wave attack (NWP), (ii) Overtopping with wind and perpendicular wave attack (iii) Overtopping with no wind and oblique wave attack (NWO) and (iv) Overtopping with wind and oblique wave attack (WWO). Sketch illustrates why oblique wave attack (lower panels) may cause a smaller influence of wind than perpendicular wave attack (upper panels).

2 Physical model tests

2.1 Test set-up

The physical model testing followed all provisions of typical wave overtopping campaigns at breakwaters such as the presence of a wave paddle in the basin that forced the irregular wave field, wave gauges placed near the toe of the structure to measure the incoming wave height, an overtopping chute and an overtopping box, etc. (see for instance Figure 2, where a simplified cross section is presented for illustration purposes). In addition to the overtopping related equipment, a paddle wheel was placed on top of the crest wall to simulate the influence of wind (see Figure 2). The experimental campaign included the testing of a rubble mound breakwater with a vertical crest wall (Figure 3) and was conducted at the Pacific Basin of Deltares (Figure 4), with effective dimensions of 14.00 m × 17.40 m. The wave board was set in motion during the experimental campaign, has a total length of 7.0 m. The second wave board present in the basin was not activated, and a dissipative rock slope was placed in front of it. A guiding (or separation) wall, 9.50 m in length, was installed between the operating and the immobile wave board to generate a uniform, long-crested wave field towards the testing section (see Figure 4).

The test section was rotated at an angle of 45 degrees to the wave direction to facilitate an oblique wave field at the structure. To effectively handle wave dissipation at the outer walls of the basin and minimise undesired reflections, dissipative slopes were placed along the side of the basin where the wave board was not activated. These dissipative sections comprised rock slopes of 1:3 and a wooden ramp with a slope of 1:2.2. Opposite the wave board, the basin's internal wall was constructed using gabions.

Tests were performed with a uniform flat bed in the basin, without wave breaking occurring on the foreshore. The incoming wave signal near the toe of the structure was measured using an array of three resistance wave gauges (WHM01-03 in Figure 4) placed in the vicinity of the structure, and the methodology of Zelt and Skjelbreia (1992) was used to separate the incoming and reflected wave fields. In addition, a directional wave gauge (GRSM in Figure 4) was placed in the basin to check the method to obtain the incident waves. Continuous measurements of overtopping discharges were taken at one cross-section by attaching an overtopping chute to the crest wall, which guided the overtopping water into a container where the water level was recorded. To measure the overtopping discharge, two resistance gauges were placed inside the overtopping collection boxes, located on the leeside of the breakwater. The overtopping box comprised two separate chambers. During a wave simulation, the first chamber was initially filled with water that had overtopped the structure, until the water level in this chamber reached a defined upper threshold. At that point, measurements in the second chamber were automatically activated, allowing the storage and recording of additional overtopping volumes. When the second, and largest, chamber was also filled with water, the pumping system was triggered automatically to empty the second chamber.

The test section comprised a rubble mound breakwater with a crest wall element placed on top of the armour crest (Figure 3). The armour layer of the breakwater was stabilised by applying epoxy to prevent movement of the stones during wave simulations, while maintaining the structure's permeability. The seaward slope of the rubble mound structure was 1:3, with the armour crest reaching a maximum elevation of 0.90 m above the bottom of the basin. The armour crest width in front of the crest wall was G_c = 0.15 m.

Two vertical crest wall elements of varying heights were tested consecutively, with protruding parts corresponding to h_c = 0.05 m and h_c = 0.08 m, respectively. The landward slope of the breakwater was 1:1.5. The breakwater has a typical cross-section consisting of an armour layer, filter layer and core. The thickness of the armour layer was $2D_{n50,a}$, with $D_{n50,a}$ = 38.5 mm, the thickness of the filter layer was d_{filter} = 36 mm, with $D_{n50,f}$ = 16.8 mm (Table 1). The core material was $D_{n50,c}$ = 6.5 mm. The total length of the cross-section, measured at the toe of the structure, was 10.60 m. Geometrical parameters of the breakwater are shown in Table 2.

In total, more than 200 tests were performed. Each wave simulation in the basin comprised an irregular wave series of approximately 1000 waves. Each random sea state followed a JONSWAP spectrum with a peak enhancement factor of γ = 3.3. In total, four water levels were tested: h = 0.70, 0.75, 0.80 and 0.85 m — with the latter tested only in combination with the highest crest wall. The selection of the range of water levels was based on two criteria: i) the water level should be high enough so that for the lowest selected H_{m0}, there is at least one overtopping event, and ii) the water level should be low enough so that the water on the leeside can have enough time to recirculate at the main compartment of the basin; these water levels were selected via sensitivity tests in the basin. Similar sensitivity tests were performed for the lower and upper bounds of H_{m0}. Wave steepness values tested were $s_{m-1,0}$ = 0.013, 0.018, 0.028 and 0.042 (see Table 3) and were pre-selected based on previous studies on the influence of wind and wave overtopping under oblique wave attack (Van Gent et al., 2024 and Van Gent and Van der Werf, 2019). This test programme was selected to obtain results that cover a wide range of relevant wave and wave overtopping conditions and various combinations of water levels and wave heights were made to create a wide range of H_{m0}/h_c and R_c/H_{m0}. An overview of the test programme is given in Table 3.

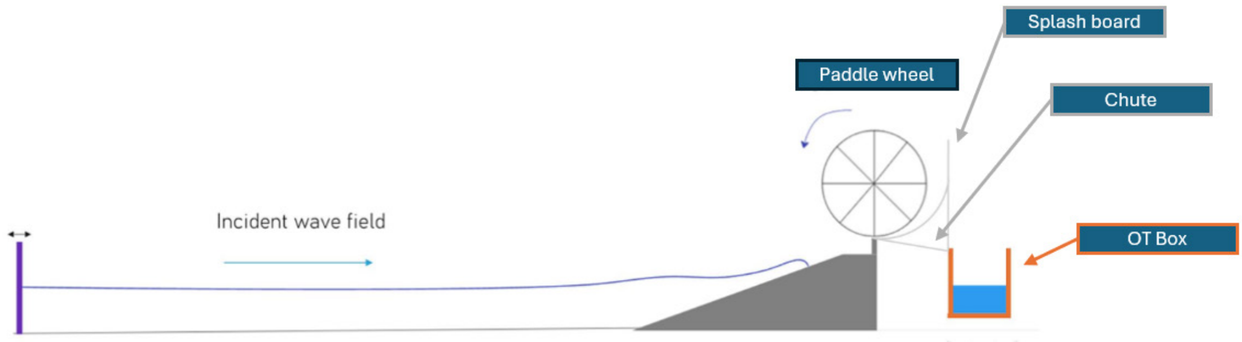

Figure 2: Conceptual sketch of the wave flume with coastal structure and paddle wheel on top of the crest wall. On the right-hand side of the flume, there is the equipment related to overtopping measurements: a splash board that prevents water droplets from spreading outside the measurement box, an overtopping chute that collects and guides the water from the measurement cross section, and the overtopping (OT) box, where the water level is gauged with resistance type probes.

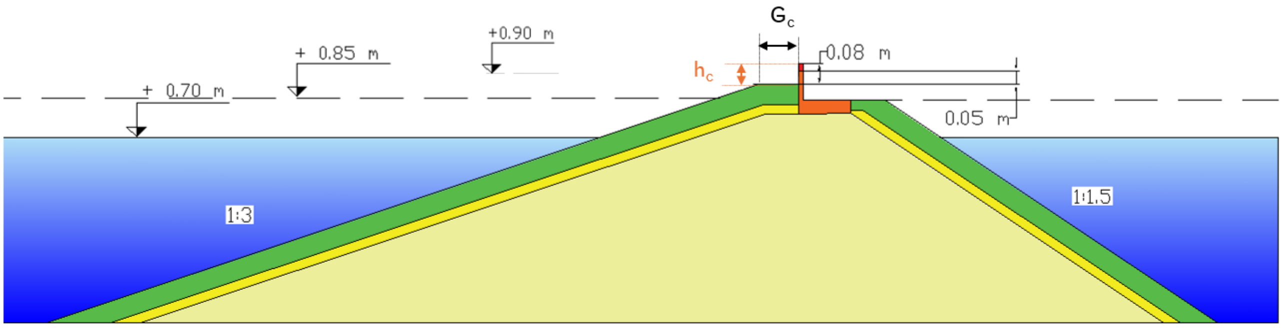

Figure 3: Test section of rubble mound breakwater with crest wall element. Indicating: water level tested range +0.70 m to +0.85 m, armour crest level at +0.90 m. Additional geometric parameters: Armour crest width G_c = 0.15 m, protruding part of the crest wall tested, h_c = 0.05 and 0.08 m.

2.2 Method to assess the maximum effect of wind on overtopping

This study employed the approach of De Waal et al. (1996) to assess the maximum influence of wind on wave overtopping discharge by means of a rotating paddle wheel. Previous studies (Wolters and Van Gent, 2007; Van Gent et al., 2025) optimised and applied this experimental method for use with dikes and breakwaters featuring crest wall elements, under condition of normal wave incidence. In this study, this approach was applied to estimate the maximum wind effect under oblique wave incidence. The paddle wheel structure is shown in Figures 5 and 6.

The paddle wheel is a wooden structure comprising 12 paddles intersecting three circular discs, two on the outer sides and one in the middle. The diameter of the circular disc is 1.4 m. The paddle wheel was mounted on a metal frame anchored inside the breakwater, ensuring it remained securely in position during wave testing. During the reference wave overtopping tests, the paddle wheel was lifted so that the waves could overtop without any obstruction, thus recording ‘reference’ values of mean overtopping discharge without wind. Subsequently, a second part of the campaign was carried out in which the paddle wheel was lowered to the topmost level of the crest wall element, with a vertical offset just sufficient to allow its free rotation. This configuration was used for assessing the maximum influence of wind, as shown in Figure 7. The rotation of the paddle wheel was motor driven and calibrated at 22 rotations per minute.

Each test condition was performed twice, once with and once without the rotating paddle wheel, using the same wave steering file. This ensured that the maximum influence of wind, measured as the ratio of overtopping during the test with and the test without the rotating paddle wheel, was isolated. In other words, there was no variation of the simulated wave trains between both tests. As a result, if the recorded discharge timeseries of a given hydraulic boundary condition is overlapped for both with and no-wind conditions, the overtopping events should occur simultaneously.

Visual observations during the tests without the rotating paddle wheel showed that under combination with low overtopping discharges, the runup wedge more frequently produced a vertical splash of water (see Figure 8). This upward motion occurred as the wave collapsed against the crest wall. This volume of water typically fell back seawards of the crest wall. However, in the presence of wind, this water can be transported onshore. In contrast, during test conditions with severe wave overtopping, larger amounts of water overtopped with minimal vertical splash.

In a limited number of tests, the test with the rotating paddle wheel, the mean overtopping discharge was observed to be somewhat less than the corresponding test without the rotating paddle wheel. To investigate this, one such test was repeated four times with the paddle wheel positioned on the crest wall. In every repetition, the mean discharge remained consistently lower than in the reference test, confirming the presence of a model effect. A few tests conducted with relatively small wave heights also yielded discharges that were lower for the test with the rotating paddle wheel than the corresponding tests without the rotating paddle wheel. This is likely due to the extremely low overtopping volumes in these cases, which are inherently difficult to reproduce and prone to scale effects. Conditions leading to influence factors below one were excluded from the analysis.

Table 1: Material information for test section, grain size and gradings.

	Nominal Diameter D_{n50} (mm)	Grading (d_{85}/d_{15})	Layer thickness (mm)
Armour Layer	38.5	1.37	77
Filter Layer	16.8	2.03	36
Core	6.5	1.62	–

Table 2: Dimensions and geometry of test section.

Parameter	Symbol	Value range
Protruding part of crest wall [m]	h_c	0.05 and 0.08
Level of armour crest w.r.t. still water level [m]	A_c	0.05 – 0.20
Crest Freeboard [m]	R_c	0.13 – 0.28
Seaward slope [-]	cot α	3
Wave angle of incidence [°]	β	45
Armour crest width [m]	G_c	0.15

Table 3: Hydraulic boundary conditions measured at the toe of the structure.

Parameter	Symbol	Value range
Significant wave height [m]	H_{m0}	0.068 – 0.16
Peak wave period [s]	T_p	1.23 – 2.97
Spectral mean wave period [s]	$T_{m-1,0}$	1.12 – 2.7
Water depth [m]	h	0.70, 0.75, 0.80, 0.85
Wave steepness [-]	$s_{m-1,0}$	0.013 – 0.042
Breaker parameter [-]	$\xi_{m-1,0}$	1.63 – 2.92

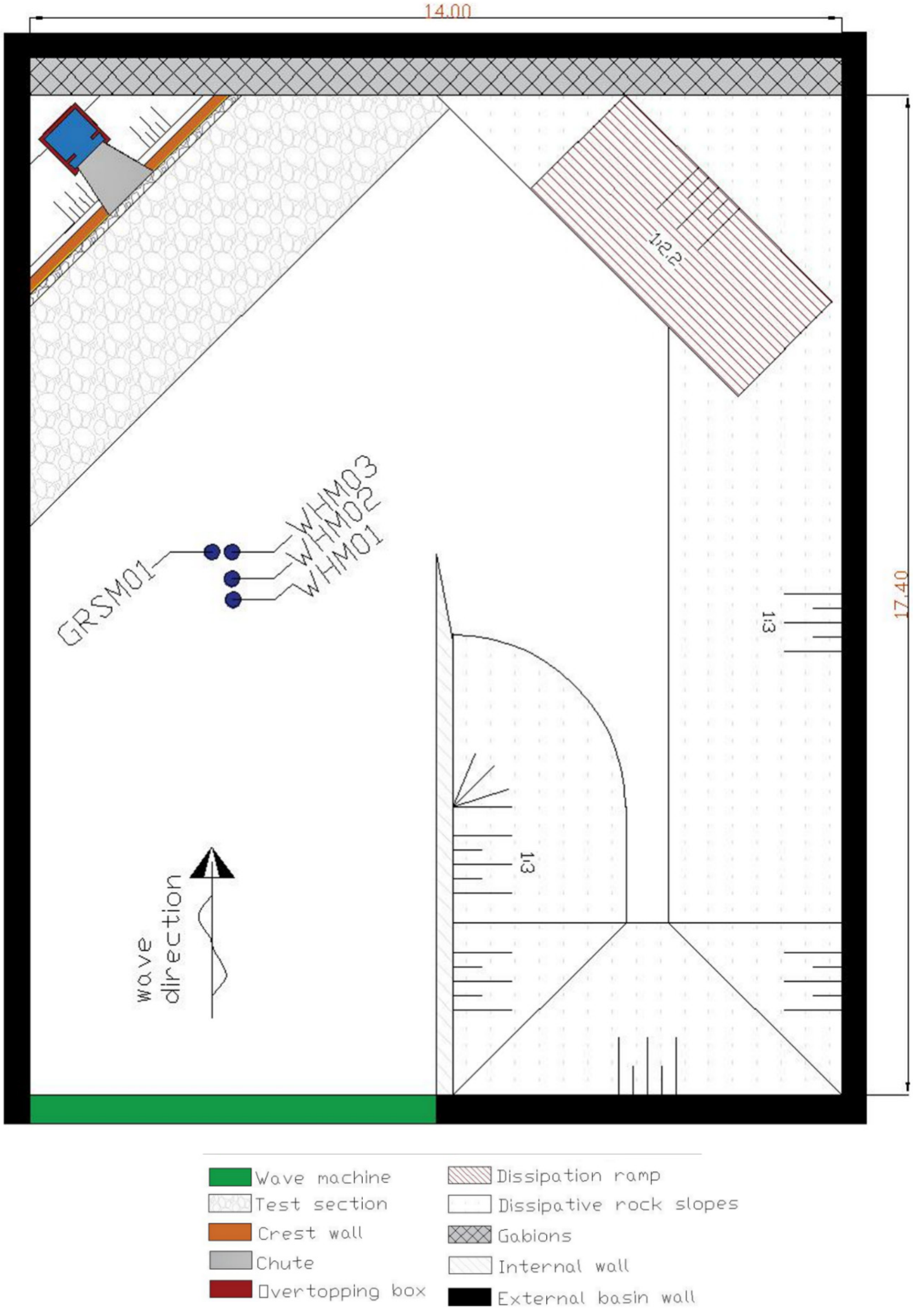

Figure 4: Experimental setup in the Pacific Basin of Deltares. The wave board is shown in green together with the wave direction. The test section of the rubble mound breakwater, crest wall element, dissipation slopes, ramp and gabions, overtopping box, directional wave gauge (GRSM01, consisting of a wave gauge and velocity meter) and wave height meters (WHM01-03) are also illustrated. All dimensions are expressed in meters.

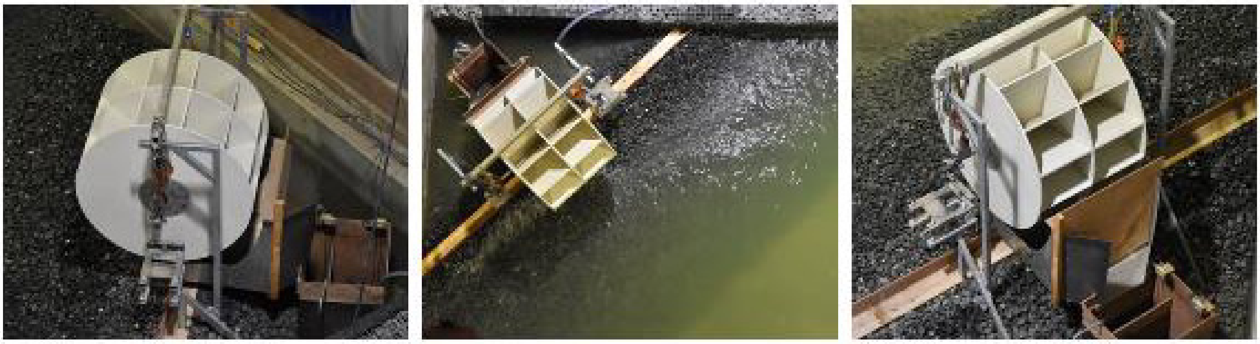

Figure 5: Test section configuration including the paddle wheel, seen from various angles.

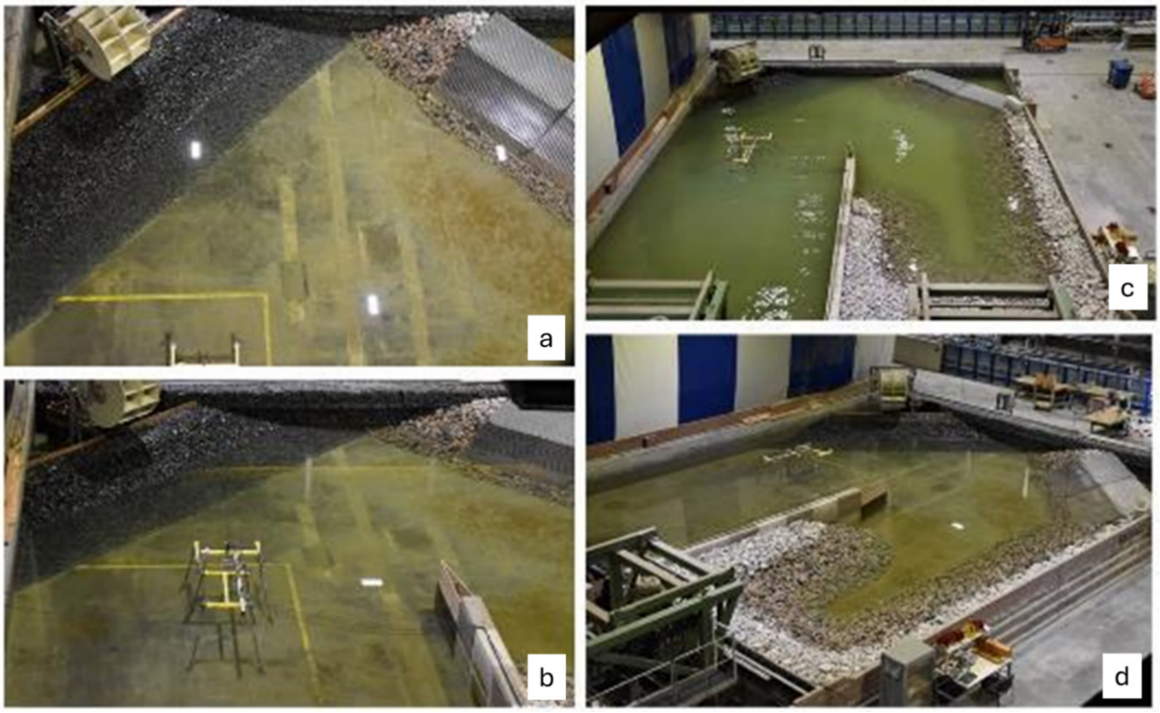

Figure 6: Experimental setup in basin. Photos taken from above the basin: (a) Plan view of the test cross section on the left and the dissipative slope on the right. (b) Plan view focusing on the measurement station, on which the wave height meters were mounted; station is located at the toe of the breakwater. (c) Oblique view of the basin showing the wave generator and generation zone on the left and dissipative slopes on the right. (d) Oblique view of the basin from a different angle, showing monitoring station and dissipative slopes.

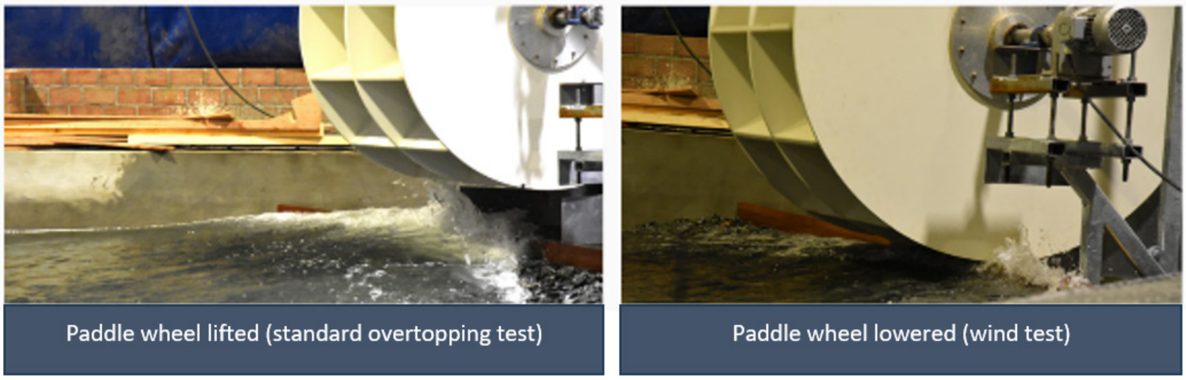

Figure 7: Test section configuration, during reference overtopping test (left panel) and during test with rotating paddle wheel (right panel).

Figure 8: Top panel: Low steepness waves. Mid-panel: High steepness wave breaks on the seaward slope. Lower left panel: Wave overtopping creating vertical splash above the crest wall. Lower right panel: Severe wave overtopping violently attacking the leeside amour slope after a wave runs over the crest wall.

3 Analysis of test results

3.1 Maximum influence of wind on wave overtopping discharges

A first overview of the results regarding the mean overtopping discharge as a function of the relative freeboard for various steepness values is presented in Figure 9, for both the lower (h_c = 0.05 m) and higher crest wall (h_c = 0.08 m) tested. The results show a negative correlation between dimensionless discharge and relative crest freeboard. At the same time, the data are stratified by wave steepness; the steeper the waves, the more rapidly the mean overtopping decreases with increasing relative freeboard. Therefore, the test results confirm, see also Irías Mata and Van Gent (2023) and Van Gent *et al.* (2025), that for waves of the same wave height, wave overtopping at rubble mound structures increases significantly with increasing wave period.

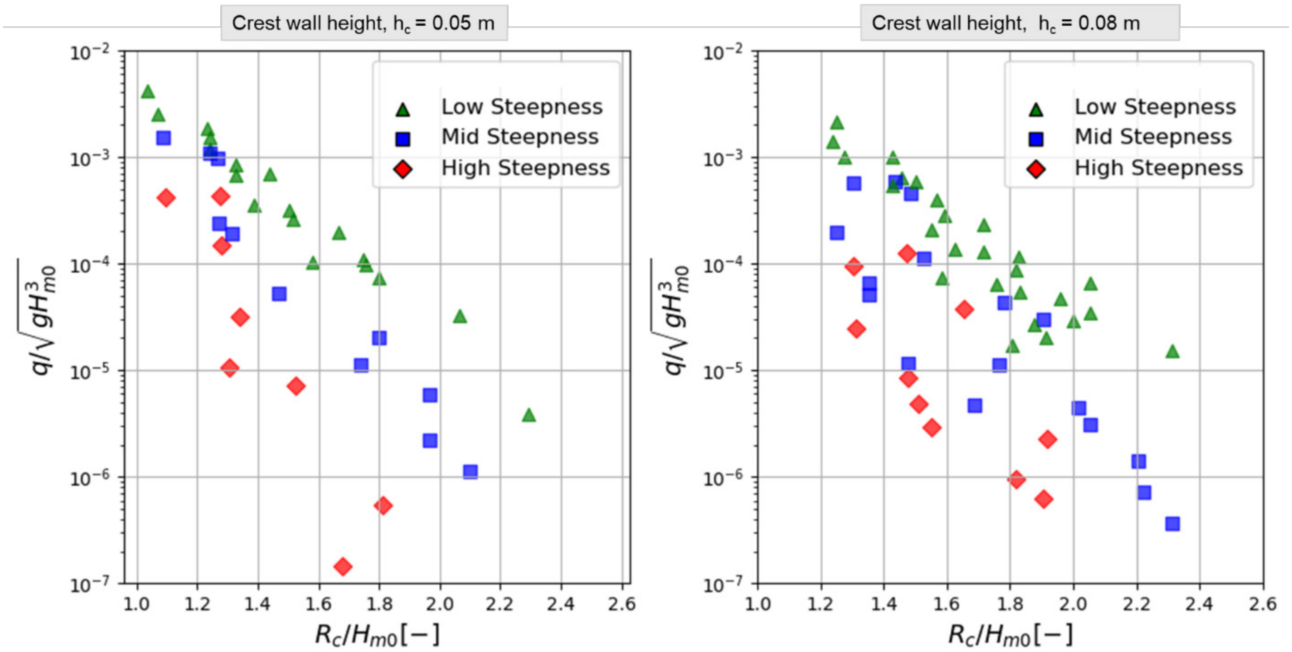

Figure 9: Dimensionless overtopping discharge versus relative freeboard. Left panel: Low crest wall, with protruding part h_c = 0.05 m. Right panel: High crest wall, with protruding part, h_c = 0.08 m. Low steepness values correspond to $s_{m\ 1,0}$ = 0.013 and 0.018, mid steepness corresponds to $s_{m-1,0}$ = 0.028 and high steepness corresponds to $s_{m-1,0}$ = 0.042.

The wind influence factor is calculated as the ratio of the discharge measured during the tests with and without the rotating paddle wheel:

$$\gamma_w = \frac{q^*_{with\ wind}}{q^*_{without\ wind}} \tag{2}$$

It is important to note that the definition provided in Eq.2 is equivalent to the ratio of dimensional discharges, since the same wave height is used to obtain non-dimensional values. The results presented in Figure 10 show the wind influence factor, γ_w, calculated using Eq.2. The two largest measured wind influence factors were γ_w = 4.3 (with q^* = $1.5 \cdot 10^{-7}$) and γ_w =3.2 (with q^* = $1.1 \cdot 10^{-6}$). Wave overtopping discharges smaller than q^* = $1 \cdot 10^{-6}$ are often less relevant and scale effects may be present.

Figure 10 also shows how the data points are distributed with respect to wave steepness. Four target steepness values were tested: $s_{m-1,0}$ = 0.013, 0.018, 0.028, and 0.042. In Figure 10, the two lower steepness values are grouped as ‘low steepness’, while $s_{m-1,0}$ = 0.028 is classified as ‘mid-steepness’, and $s_{m-1,0}$ = 0.042 as ‘high steepness’. The dataset does not display a clear stratification by wave steepness. Therefore, a clear dependency of the wind influence factor on steepness is not present; the influence of the wave steepness on wave overtopping is similar for the tests with and without the rotating paddle wheel and no additional influence of the wave steepness is present in the wind influence factor.

In the right panel of Figure 10, the wind influence factor γ_w is plotted against the relative freeboard. The results show that, for all wave steepness values, the relative freeboard is positively correlated with the wind influence factor. Analysis of the dataset reveals that, for a given incident significant wave height (and water depth), a higher wave steepness corresponds to a shorter wave period, which in turn leads to lower overtopping discharges. It has already been shown that higher wind influence factors occur in the low overtopping regime. This is evident in the left panel of Figure 10, where data points corresponding to lower steepness values appear predominantly in the higher overtopping discharge range.

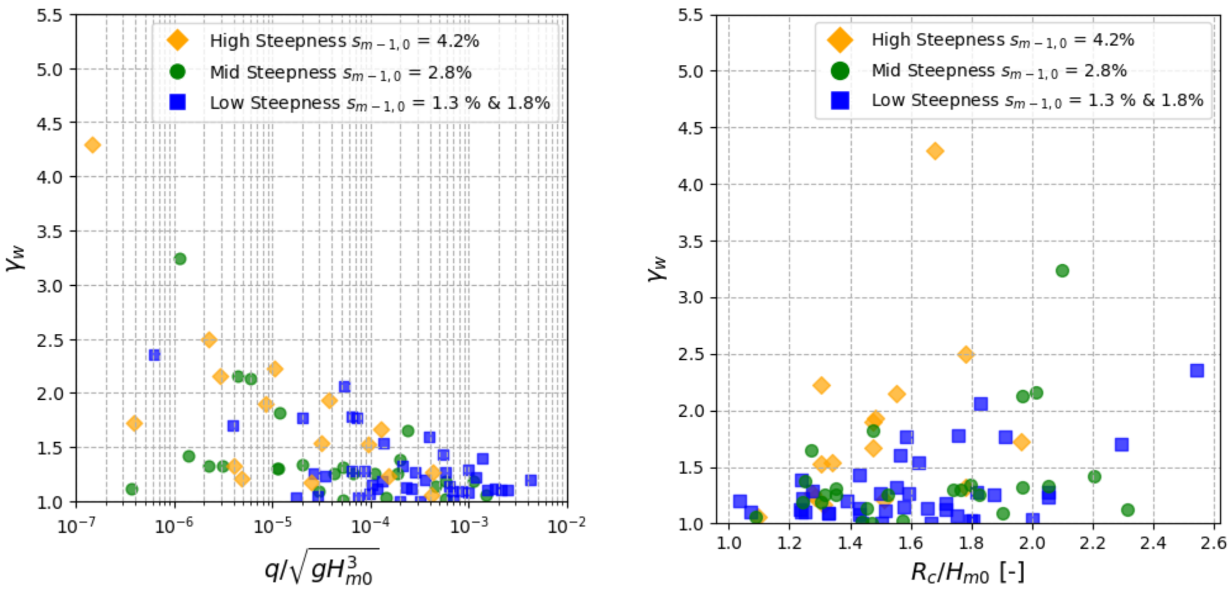

Figure 10: Wind influence factor γ_w versus mean overtopping discharge in tests without the paddle wheel (left panel) and relative freeboard R_c / H_{m0} (right panel).

The data from the present tests are again plotted in the left panel of Figure 11, now for the relevant range with discharges larger than $q^* = 1 \cdot 10^{-6}$. The most recent expression to predict the maximum influence of wind on wave overtopping (Eq.1) has been developed based on conditions with perpendicular wave attack. The dashed curve in the left panel of Figure 11 corresponds to Eq.1. The graph shows that for the present tests with oblique wave attack the maximum influence of wind on wave overtopping is generally smaller than Eq.1 for perpendicular wave attack. This comparison indicates that the effect of oblique wave attack on the influence factor for wind needs to be incorporated in the prediction method. Therefore, an extension to Eq.1 is proposed to account for oblique wave incidence. Use is made of the expression that was also used to account for effects of oblique waves on the stability of armour units, forces on crest walls and on wave overtopping (e.g. Van Gent, 2014; Van Gent and Van der Werf, 2019; Van Gent, 2022):

$$\gamma_\beta = (1 - c_\beta) \cos^2\beta + c_\beta \tag{3}$$

The expression proposed in Van Gent (2022) leads to $c_\beta = 0.3$ for a 1:3 rubble mound slope. Eq.1 is extended to Eq.4 in which the power 2.5 is calibrated based on the present data-set. This results in an expression for the maximum influence of wind on wave overtopping that not only account for the protruding height of the crest wall (non-dimensional ratio h_c / H_{m0}) but also for the influence of oblique waves on the maximum effects of wind:

$$\gamma_w = 1 + 0.075\, {\gamma_\beta}^{2.5} \frac{h_c}{H_{m0}} (q^*)^{-0.3} \tag{4}$$

This expression for non-dimensional discharges larger than $q^* = 1 \cdot 10^{-6}$ results in a maximum influence of wind on wave overtopping discharges for perpendicular waves ($\beta = 0°$ and $\gamma_\beta = 1$) and in no influence of wind for a non-protruding crest wall ($h_c = 0$). The extended expression (Eq.4) is illustrated by the red curve in the left panel of Figure 11.

In the present data-set with and angle of incidence of $\beta = 45°$ Eq.3 provides $\gamma_\beta = 0.65$. Eq.4 yields an RMSLE of 0.103 (see Eq.5. for the applied expression; based on conditions with $q^* \geq 1 \cdot 10^{-6}$ and $\gamma_w \geq 1$) when comparing measured versus predicted discharges under the maximum influence of wind, as shown in the right panel of Figure 11 (q^*_{wind} -predicted = $\gamma_{w\,(\text{Eq.4})} \cdot q^*_{measured\text{ - }no\ wind}$ versus $q^*_{measured\text{ - }with\ wind}$). The match between the expression and the data is reasonably good but it is recommended to verify the validity of Eq.4 also for other angles of wave incidence. Nevertheless, Eq.4 is expected to provide a reasonably estimate for other angles of wave incidence due to the similarity of the expression for other processes depending on the angle of wave incidence. Note that all data from the present test programme has been used to calibrate the power 2.5 in Eq.4. Eq.4 provides first estimates also for wave angles between perpendicular wave attack ($\beta = 0°$) and the tested wave angle ($\beta = 45°$).

$$\text{RMSLE} = \sqrt{\frac{\sum_{i=1}^{n_{tests}} \left(log(q*_{measured}) - log(q*_{calculated})\right)^2}{n_{tests}}} \tag{5}$$

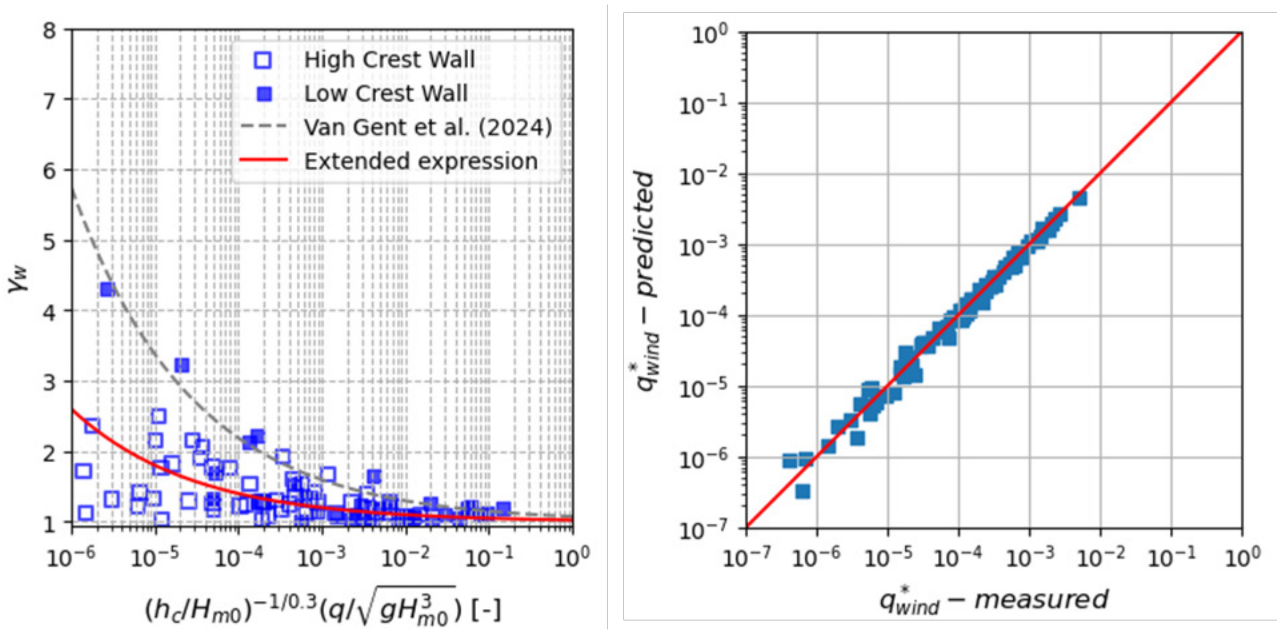

Figure 11: Left panel: Present data ($q^* > 1.0 \cdot 10^{-6}$) compared to the original expression (dashed curve; Eq.1) and extended expression (red curve; Eq.4). Right panel: Predicted and measured wave overtopping discharges under the influence of wind, based on newly proposed Eq.4.

3.2 Maximum influence of wind on volumes in wave overtopping events

The experimental research has shown that the wind influence factor largely depends on the overtopping discharge, exhibiting a strong effect in the low discharge regime and a diminishing influence as the discharge increases. To the best of the authors' knowledge, no existing studies have quantified the extent of this declining wind influence relative to the overtopping volumes of individual wave overtopping events. Analysis of the present dataset by isolating the volumes within individual overtopping events V and calculating the ratio of overtopping volumes with and without the rotating paddle wheel provides estimates of the maximum influence factor for individual overtopping volumes:

$$\gamma_{w-Vol} = \frac{V_{with\ wind}}{V_{without\ wind}} \tag{6}$$

Where the ratio $V_{with\ wind}$ and $V_{without\ wind}$ is determined for overtopping events for which $V_{without\ wind} > 1.0{\cdot}10^{-4}$ m^3/m. Identifying overtopping volumes from individual overtopping events in physical model tests is known to be challenging. In this experimental setup, separating overtopping events is based solely on a typical overtopping measurement technique with water level probes placed inside the overtopping box. In a few tests, particularly for those in the high overtopping regime, consecutive waves overtopped in a manner that yields separation of volumes attributed to each overtopping wave impossible. This occurs because the overtopping flow from the chute to the collection box due to the first wave has not yet stopped when a second wave follows up and accumulates in the overtopping chute. A steeper gradient of the acquired elevation timeseries measured inside the overtopping box indicates an overtopping volume added into the container. The selection of this gradient has shown to be a critical factor for the analysis, that can potentially lead to detection of too many events (for a low threshold gradient) or too few events (high threshold gradient). The threshold applied herein to separate overtopping events was $1.0{\cdot}10^{-4}$ m^3/m and a declustering time, which is used to separate two consecutive events, of five seconds.

The tests showed, see also Figure 12, that the maximum influence of wind on volumes within individual wave overtopping events is large for small volumes and negligible for large volumes. The largest measured influence factor for individual overtopping events seems to be roughly a factor two greater than the largest measured influence factor for mean overtopping discharge. A few values of $\gamma_{w\text{-}Vol}$ greater than 10 appeared in the data analysis, but these are considered to be a result of very small volumes and related instrument-induced noise in the recording of overtopping volumes. The above described separation technique to distinguish between two consecutive overtopping events with large volumes occurring quickly after each other, is especially relevant for conditions with a lot of overtopping, but for these conditions the influence of wind is relatively small. Therefore, the separation technique is considered less critical for determining the maximum influence of wind on volumes within individual overtopping events.

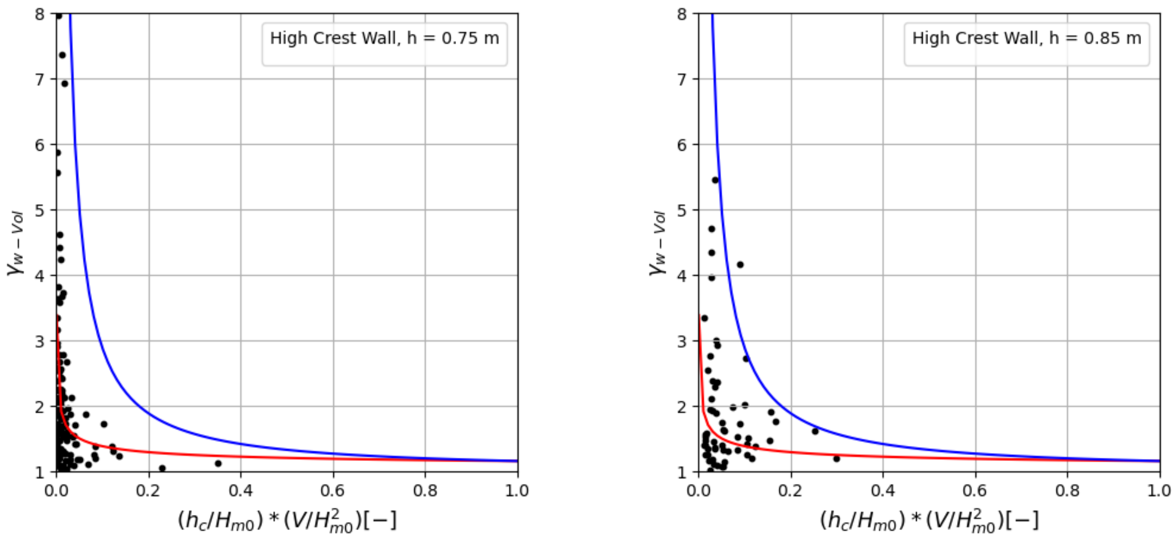

Figure 12: Wind influence factor for volumes $V_{without\ wind}$ in individual overtopping events $\gamma_{w\text{-}Vol}$ versus the non-dimensional overtopping volumes $V_{without\ wind}/H_{m0}^2$ times the non-dimensional protruding part of the crest wall (h_c/H_{m0}); Left panel: High crest wall, h_c = 0.08 m, water level, h = 0.75 m. Right panel: High crest wall, h_c = 0.08 m, water level, h = 0.85 m.

A new expression is proposed for a wind influence factor $\gamma_{w\text{-}Vol}$, based this time on overtopping volumes instead of the discharge, so as to predict the overtopping volume of an individual overtopping event under the maximum influence of wind:

$$\gamma_{w-Vol} = 1 + a\frac{h_c}{H_{m0}}\left(\frac{V_{without\ wind}}{H_{m0}^2}\right)^{-b} \tag{7}$$

The proposed coefficients for Eq.7 are: $a = 0.15$; $b = 0.40$ for the best fit, and $a = 0.15$; $b = 1.1$ for the "upper bound", as shown in Figure 12. The "upper bound" can be used for design purposes if a conservative estimate of the influence of wind is required. Moreover, the analysis revealed that the inclusion of the protruding part of the crest wall height to wave height ratio (h_c/H_{m0}) offers a slight improvement in the prediction of the wind influence factor with respect to individual events. Note that in Eq.7 no influence of oblique incident waves has been accounted for since no data on volumes within individual wave overtopping events is available for conditions with perpendicular wave attack. If a similar approach as applied for wave overtopping discharges (Eq.4) would be adopted for volumes in overtopping events, Eq.7 would read:

$$\gamma_{w-Vol} = 1 + a'\gamma_\beta{}^c \frac{h_c}{H_{m0}} \left(\frac{V_{without\ wind}}{H_{m0}^2}\right)^{-b} \tag{8}$$

The proposed coefficients for Eq.8 are: $a' = 0.44$, $b = 0.40$ and $c = 2.5$ for the best fit, and $a' = 0.44$, $b = 1.1$ and $c = 2.5$ for the "upper bound". However, since no data for volumes in overtopping events under perpendicular wave attack is available, Eq.8 still needs to be validated based on such tests; especially validation of the value for the coefficient c is required.

4 Discussion

The tests consistently show that the maximum influence of wind on wave overtopping is less for oblique wave conditions than for perpendicular wave attack. For lower discharges, for which the influence of wind is relatively large, the crest wall causes a vertical motion of water into the air. Without wind a part of this water overtops and a part falls back to a position seaward of the crest wall. With wind a larger part of the water in the air is transported over the crest wall. The water droplets ejected in the air, do not necessarily remain at exactly the same cross-section but are somewhat re-distributed in the longitudinal direction (see lower left panel of Figure 8 in a photo taken during the experiments). This redistribution of droplets in the vicinity of the crest wall is conceptualised in the two illustrations of Figure 13. In the left panel of Figure 13, the randomly allocated droplets can be visually grouped based on their distance to the crest wall being either relatively small (Δx_1, shown with the blue arrow) or relatively large (Δx_2, shown with the arrow red color). This qualitative separation of points can be further visualized through the right panel of Figure 13, where the blue plane shows potential locations of the sum of droplets above the crest wall that are eventually more likely to overtop, while the red plane shows the location of droplets that are less likely to overtop even under the influence of wind.

Further elaborating on the observations and assumptions that were visualized above, it can be hypothesized that in the case of oblique waves, about half of the water distributed in the longitudinal direction is more easily transported over the crest since at those locations the crest wall is positioned more seaward ("crest wall relatively seaward") compared to the original position, while half of the distributed water ends up in positions for which the crest wall is positioned more landward ("crest wall relatively landward") compared to the original position. For the latter half ("crest wall relatively landward"), the wind has to transport the water over a slightly larger distance to cause overtopping. For the other half ("crest wall relatively seaward"), the water would overtop also without the presence of wind. The net result would be that a longitudinal re-distribution of water would cause that half of the water needs to be transported by wind over a slightly larger distance than without a longitudinal distribution. Based on the above, it can be inferred that this causes the reduction of the maximum effect of wind in case of oblique waves.

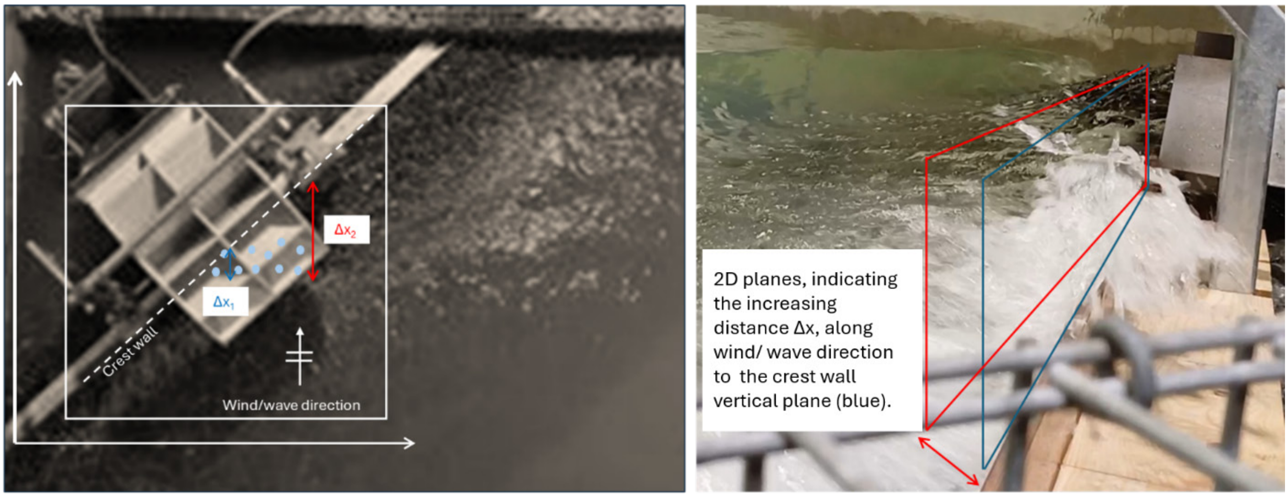

Figure 13: Conceptual schematic views supporting discussion of wind effects under oblique wave attack. Left panel: Top view of experimental setup showing the distance relative to the crest wall that a droplet has to cross to reach the crest wall and overtop after wave breaking on the vertical front of crest wall element. Right panel: Two representative 2D planes are shown. The plane with the blue outline is closer to the crest wall (most of water in this area will overtop under the influence of wind) and the plane with the red outline (clockwise rotated compared to the blue one) which is located farther from the crest wall (water droplets in this area are less likely to be transported onshore and overtop under the wind influence when oblique waves attack the structure).

5. Conclusions and recommendations

The effect of wind on wave overtopping at rubble mound breakwaters with crest walls can be significant and cannot be neglected, especially in low discharge regimes where onshore wind can substantially increase overtopping. Accurately capturing wind influence in physical models poses challenges due to the incompatibility of Froude scaling with wind dynamics. This study, supported by a comprehensive experimental campaign, proposes a methodology to estimate the maximum wind influence on overtopping at rubble mound breakwaters with vertical crest wall elements. Findings indicate that the maximum wind-induced increase in overtopping discharges diminishes under oblique wave incidence compared to perpendicular wave attack. The presence of a vertical crest wall plays a critical role in enhancing overtopping under wind influence, as the upward splash following wave impact on the wall facilitates additional water transport onshore. Main conclusions of this study are summarised below:

- The experimental data from this campaign confirm existing theoretical assumptions and previous findings that the wind influence on wave overtopping decreases as the overtopping discharge increases. Consequently, the most significant wind effect occurs in the low discharge regime for both normal and oblique wave incidence.
- Measurements show that mean overtopping discharge can increase by up to a factor of 4.3 under onshore wind conditions at rubble mound breakwaters with vertical crest wall elements during oblique wave attack.
- An extended prediction formula (Eq.4) is proposed to quantify the maximum effect of wind on overtopping discharges. The wind influence factor (γ_w) correlates positively with the vertical crest wall height (h_c), negatively with overtopping discharge (q), and negatively with the angle of wave incidence (β). This formula can be applied directly to mean overtopping discharges derived from physical or numerical models, data-driven machine learning tools, or empirical relations that quantify wave overtopping discharges in absence of wind.
- Analysis of individual overtopping volumes reveals that the wind influence factor exhibits similar trends to that based on mean discharge, *i.e.*, γ_w is larger for smaller overtopping volumes and decreases as volumes increase. This is attributed to spray-like behaviour with significant upward water motion during less severe events, versus a "green-water" overtopping dominated by broken wave fronts running over the crest wall during heavy overtopping. Eqs.7 and 8 can provide first estimates to account for the influence of wind on volumes within individual wave overtopping discharges, but these expressions need to be validated based on additional data, especially for perpendicular wave attack.

- The proposed modelling methodology to account for the potential influence of wind does not require explicit scaling laws for wind forcing, as it accounts for the maximum wind effect directly, eliminating the need to upscale wind conditions in physical models.

To further validate and extend the applicability of the proposed formula and findings, it is recommended to *a)* test a broader range of wave angles of incidence in addition to the tested angle of incidence of 45°, *b)* investigate different crest wall configurations in addition to the tested vertical crest walls, and *c)* investigate the influence of wind on the distribution of volumes, water layer thickness, and velocities of individual overtopping events. The main recommendation is to account for wind in the design of rubble mound breakwaters, using Eq.4 to account for wind, and adjust the height of the structure, mitigating the increased wave overtopping discharge due to wind.

Acknowledgements

The assistance by Wesley Stet, Peter Alberts and Danny van Doeveren (Deltares) during the physical model tests is highly appreciated. Marisol Irías Mata (Deltares) and Davide Wüthrich (Delft University of Technology) are acknowledged for their participation in the supervision of the described study.

Funding

This study was realized with the support by the ‘Vereniging van Waterbouwers’ and by the Deltares’ Strategic Research Program Resilient Infrastructure (MS5.5).

Author contributions (CRediT)

MS: Investigation, Data curation, Formal analysis, Visualisation, Writing-original draft; MvG: Conceptualisation, Methodology, Investigation, Writing-Reviewing & editing, Funding acquisition, Supervision.

Use of AI

No AI was used in the preparation of this work.

Data access statement

The new data acquired in the study will be made available on request (license CC-BY-NC-SA).

Declaration of interests

There is no conflict of interest.

Notation

Name	Symbol	Unit
influence factor for wave overtopping	γ	-
crest level of armour at crest, relative to still water level	A_c	m
stone diameter	D_{n50}	m
significant wave height of incident waves at toe of structures, based on wave energy spectrum	H_{m0}	m
water depth	h	m
height of the crest wall above the level of the armour at the crest ($h_c = R_c - A_c$)	h_c	m
mean overtopping discharge	q	$m^3/s/m$
non-dimensional mean overtopping discharge: $q^*=q/(g\ H_s^3)^{0.5}$	q^*	-
freeboard (crest height relative to still water level; negative for submerged structures)	R_c	m
wave steepness calculated using $s_{m-1,0} = 2\pi\ H_{m0} / gT_{m-1,0}^2$	$s_{m-1,0}$	-
spectral mean wave period of the incident waves	$T_{m-1,0}$	s
volume of water in an individual wave overtopping event	V	m^3/m

References

Baines, A., L.S. Cunningham, and B.D. Rogers (2024): Shore-side downfall pressures due to waves impacting a vertical seawall: an experimental study. *Journal of Marine Science and Engineering, 12(12),* Article 2149. https://doi.org/10.3390/jmse12122149

Chen, W., J.J. Warmink, M.R.A. van Gent, and S.J.M.H. Hulscher (2021): Numerical modelling of wave overtopping at dikes using OpenFOAM®. *Coastal Engineering*, *166*, Article 103890. https://doi.org/10.1016/j.coastaleng.2021.103890

Chen, W., J.J. Warmink, M.R.A. van Gent, and S.J.M.H. Hulscher (2022): Numerical investigation of the effects of roughness, a berm and oblique waves on wave overtopping processes at dikes. *Applied Ocean Research*, *118.* https://doi.org/10.1016/j.apor.2021.102971

Chen, X., I. Riviera-Arreba, and B. Hofland (2023): Experimental study of spray form wave impact. In K. Burgess (Ed.), *Coasts, Marine Structures and Breakwaters 2023: Resilience and adaptability in a changing climate*. Emerald Publishing.

Den Bieman, J.P., M.R.A. van Gent, and H.F.P. van den Boogaard (2021): Wave overtopping predictions using an advanced machine learning technique. *Coastal Engineering, 166,* Article 103830. https://doi.org/10.1016/j.coastaleng.2020.103830

De Ridder, M.P., D.C.P. van Kester, R. van Bentem, D.Y.Y. Teng, and M.R.A. van Gent (2024): Wave overtopping discharges at rubble mound structures in shallow water. *Coastal Engineering*, *194*, Article 104626. https://doi.org/10.1016/j.coastaleng.2024.104626

De Waal, J.P., P. Tönjes, and J.W. van der Meer (1996): Wave overtopping of vertical structures including wind effect. *Proc. ICCE 1996 conference*, *1*(25), 172.

Di Leo, A., F. Dentale, M. Buccino, S. Tuozzo, and E.P. Carratelli (2022): Numerical analysis of wind effect on wave overtopping on a vertical seawall. *Water*, *14*(23), Article 3816. https://doi.org/10.3390/w14233891

Eldrup, M.R., T. Lykke Andersen, K. van Doorslaer, and J.W. van der Meer (2022): Improved guidance on roughness and crest width in overtopping of rubble mound structures along EurOtop. *Coastal Engineering*, *176*, Article 104149. https://doi.org/10.1016/j.coastaleng.2022.104152

EurOtop (2018): *Manual on wave overtopping of sea defences and related structures.* (J.W. van der Meer, N.W.H. Allsop, T. Bruce, J. de Rouck, A. Kortenhaus, T. Pullen, H. Schüttrumpf, P. Troch, and B. Zanuttigh Eds., 2nd ed. incl. Errata November 2019). overtopping-manual.com

Goda, Y. (1985). *Random seas and design of maritime structures*. University of Tokyo Press.

Goda, Y. (2010). *Random seas and design of maritime structures* (3rd ed., Vol. 33; Advanced Series on Ocean Engineering). World Scientific.

González-Escrivá, J. A. (2006). The role of wind in wave runup and overtopping of coastal structures. *Proc. ICCE 2006 conference* (25), 4766–4778. https://doi.org/10.1142/9789812709554_0399

Irías Mata, M. and M.R.A. van Gent (2023): Numerical modelling of wave overtopping discharges at rubble mound breakwaters using OpenFOAM®. *Coastal Engineering*, *181*, Article 104278. https://doi.org/10.1016/j.coastaleng.2022.104274

Jensen, O. J. (1984). *A monograph on rubble mound breakwaters*. Danish Hydraulic Institute.

Jin Y., W. Wang, C. Pákozdi, A. Kamath, and H. Bihs (2022): Numerical investigation on wave-overtopping at a double-dike defence structure in response to climate change-induced sea level rise. *Fluids*, *7*(9), Article 295. https://doi.org/10.3390/fluids7090295

Medina, J. R. (1998). Wind effects on runup and breakwater crest design. *Proc. ICCE 1998 conference* (26), 1068–1081. https://doi.org/10.1142/9789812791306_0189

Peng, Z. and Q-P. Zou (2011): Spatial distribution of wave overtopping water behind coastal structures. *Coastal Engineering*, *58*(6), 489–498. https://doi.org/10.1016/j.coastaleng.2011.01.010

Pepi, Y., A. Romano and L. Franco (2022): Wave overtopping at rubble mound breakwaters: A new method to estimate roughness factor for rock armours under non-breaking waves. *Coastal Engineering*, *173*, Article 104085. https://doi.org/10.1016/j.coastaleng.2022.104197

Shore Protection Manual (1984): U.S. Army Corps of Engineers, *Shore protection manual* (4th ed., Vol. 1–2). U.S. Government Printing Office. https://resolver.tudelft.nl/uuid:98791127-e7ae-40a1-b850-67d575fa1289

Sibul, O. J., and Tickner, E. G. (1956). *Model study of overtopping of wind-generated waves on levees with slopes 1:3 and 1:6* (Technical Memorandum No. 80). Beach Erosion Board, U.S. Army Corps of Engineers. https://apps.dtic.mil/sti/citations/tr/AD0088706

Stagnitti M., J.L. Lara, R.E. Musumeci, and E. Foti (2023): Numerical modeling of wave overtopping of damaged and upgraded rubble-mound breakwaters. *Ocean Engineering*, *281*, Article 114945. https://doi.org/10.1016/j.oceaneng.2023.114798

TAW (2002): *Technical Report: Wave Run-up and Wave Overtopping at Dikes*. Technical Advisory Committee on Flood Defence (TAW).

Van der Werf, I.M. and M.R.A. van Gent (2018): Wave overtopping over coastal structures with oblique wind and swell waves. *Journal of Marine Science and Engineering*, *6*(4), Article 149. https://doi.org/10.3390/jmse6040149

Van Gent, M.R.A., H.F.P. van den Boogaard, B. Pozueta, and J.R. Medina (2007): Neural network modelling of wave overtopping at coastal structures. *Coastal Engineering*, *54*(8), 586–593. https://doi.org/10.1016/j.coastaleng.2006.12.001

Van Gent, M.R.A. (2014): Oblique wave attack on rubble mound breakwaters. *Coastal Engineering*, *88*, 43–54. https://doi.org/10.1016/j.coastaleng.2014.02

Van Gent, M.R.A. and I.M. van der Werf (2019): Influence of oblique wave attack on wave overtopping and wave forces on rubble mound breakwater crest walls. *Coastal Engineering*, *152*, Article 103503. https://doi.org/10.1016/j.coastaleng.2019.04.001

Van Gent, M.R.A., G. Wolters, and A. Capel (2022): Wave overtopping discharges at rubble mound breakwaters including effects of a crest wall and a berm. *Coastal Engineering*, *174*, Article 104107. https://doi.org/10.1016/j.coastaleng.2022.104151

Van Gent, M.R.A. (2022): Wave overtopping at dikes and breakwaters under oblique wave attack. *Proc. ICCE 2022 conference* (37). https://doi.org/10.9753/icce.v37.papers.5

Van Gent, M.R.A., R.J. van der Bijl, S.J. Dijkstra, L.F. van Vliet, and D. Wüthrich (2024): Wind effects on wave overtopping discharges at dikes and breakwaters with a crest wall. *Proc. ICCE 2024 conference* (38). https://doi.org/10.9753/icce.v38.papers.6

Van Gent, M.R.A., J. van Marrewijk, and P. Mares-Nasarre (2025): Guidelines on wave overtopping discharges at rubble mound breakwaters including slope angle effects. *Journal of Coastal and Hydraulic Structures*, *5*, Article 48. https://doi.org/10.59490/jchs.2025.0048

Ward, D.L., C.G. Wibner, J. Zhang, and B. Edge (1994): Wind effects on runup and overtopping. *Proc. ICCE 1994 conference* (24), 2210–2224.

Ward, D.L., J. Zhang, C.G. Wibner, and C.M. Cinotto (1996): Wind effects on runup and overtopping. *Proc. ICCE 1996 conference* (25), 184–195. https://doi.org/10.1061/9780784402429.171

Wolters, G. and M.R.A. van Gent (2007): Maximum wind effect on wave overtopping of sloped coastal structures with crest elements. In L. Franco, J. Melby, & J. W. van der Meer (Eds.), *Proc. Coastal Structures conference 2007* (Vol. 1, pp. 575–586). World Scientific. https://doi.org/10.1142/9789814282024_0111

Zelt, J.A. and J.E. Skjelbreia (1992): Estimating incident waves and reflected wave fields using an arbitrary number of wave gauges. *Proc. ICCE 1992 conference* (23), 777–789. https://doi.org/10.1061/9780872629332.058